

Thermal Diffusivity and Microstructure in API5L-X52 Carbon Steel¹

G. Peña-Rodríguez,² O. Flores-Macías,³ C. Angeles-Chávez,³
J. A. I. Díaz Góngora,⁴ R. A. Muñoz-Hernández,⁴ and A. Calderón^{4,5}

The determination of the thermal diffusivity of API5L-X52 carbon steel at room temperature, by means of the photoacoustic technique in a heat transmission configuration, is reported for the first time. Since literature values of thermal diffusivity for this low carbon steel do not exist, comparisons among our thermal diffusivity (α) results for API5L-X52 steel and those reported in the literature for steels with similar compositions are reported. Moreover, a study of the microstructure of this low carbon steel by means of scanning electronic microscopy (SEM) and X-ray diffraction (XRD) is presented.

KEY WORDS: API5L-X52 carbon steel; microstructure; thermal diffusivity.

1. INTRODUCTION

A knowledge of the physical and chemical properties of materials and the relations among them is of interest in the selection of materials that will be used in the design and manufacturing of pipelines with specifications for installation, operation, and maintenance of fluid transportation. Studies of the relations between mechanical and thermal properties have been of interest to the steel and metal industries; these include studies about the

¹ Paper presented at the Fifteenth Symposium on Thermophysical Properties, June 22–27, 2003, Boulder, Colorado, U.S.A.

² Departamento de Física, Universidad Francisco de Paula Santander A. A. 1055, Cúcuta, Colombia.

³ Instituto Mexicano del Petróleo, Eje Central L. Cárdenas 152, Colonia San Bartolo Atepehuacan, 07730 México D. F.

⁴ Centro de Investigación en Ciencia Aplicada y Tecnología Avanzada del IPN, Legaria 694 Colonia Irrigación, 11500 México D. F.

⁵ To whom correspondence should be addressed. E-mail: jcalderona@ipn.mx

relation between hardness and the thermal diffusivity (α) of steel [1, 2], for example.

Thermal wave propagation in solid materials is influenced by microstructure characteristics, grain size and grain boundary, and impurities and imperfections, all of which contribute to the energy dispersion of the carriers like phonons and electrons inside the material. This energy dispersion results in a decrease in the heat flow through the material [3]. A decrease in the grain size in ferrous steel with a low carbon concentration gives an increase in the mechanical resistance of the material and thus provides better resistance to fracture [4, 5]. For these reasons and because the reported values of the thermal diffusivity for 5L specification and X52 grade are not available from the American Petroleum Institute (API) [6, 7], we have determined the thermal diffusivity of this low carbon steel at room temperature using the photoacoustic (PA) technique in a heat transmission configuration. This technique has been widely used in the thermal characterization of solids, because it offers several advantages over other methods, such as high precision measurements, small sample management, and a nondestructive technique. We can measure without direct contact, and the temperature variations inside the photoacoustic cell are small [1, 8–10]. We also did a microstructural analysis of this material using scanning electronic microscopy (SEM) and X-ray diffraction (XRD).

2. MEASUREMENTS

2.1. Specimens

We used a pipeline section, with an internal radius of 127 mm and a wall thickness of 6.35 mm, of API grade X52 carbon steel and a chemical composition (in mass percent) as follows: 0.092% C, 1.03% Mn, 0.014% P, 0.005% S, <0.005% Nb, <0.001% V, and <0.002% Ti. By means of a low-speed disc cutter (South Bay Technology SBT-650) and diamond edge discs (Buehler 11-4244), we made several cuts on the pipeline wall in order to obtain five samples of 1 cm^2 surface area and a few hundreds of micrometers of thickness for each. The sample thicknesses (l_s), shown in Table I, were accomplished using a low-speed polishing machine (SBT-910) and abrasive paper (Buehler 30-5118-240). The sample thicknesses were measured using a digital micrometer (Mitutoyo 543-252). In order to avoid oxidation of clean sample surfaces, the samples were placed in glass containers with silica gel. For metallographic processes we used $1\text{ }\mu\text{m}$ diamond paste (Buehler Metadi II) and polishing cloths (Buehler 40-7218). The structure of the material was revealed by chemical attack using a 0.2% nital solution for 10 s.

Table I. Thermal Diffusivity of API5L-X52 Carbon Steel Samples

SAMPLES	l_s (μm)	α ($10^{-3} \text{ cm}^2 \cdot \text{s}^{-1}$)
A1	167 ± 3	118 ± 5
A2	170 ± 3	116 ± 5
A3	175 ± 6	116 ± 6
A4	176 ± 3	116 ± 5
A5	170 ± 5	115 ± 6

2.2. Procedure

Since the first reports about the use of the open photoacoustic cell (OPC) for thermal characterization of solids [10], this method has been widely used in the measurement of thermal properties of a large variety of materials [8, 9]. The OPC method consists of mounting the sample under study directly onto a commercial electret microphone, while using the front chamber of the microphone as the usual gas chamber of a conventional photoacoustic technique. The main advantage over other conventional photoacoustic cells include the use of a minimal gas chamber with no further transducer medium needed, no cell machining required, and low cost.

From the one-dimensional thermal diffusion model, one obtains that the amplitude of the OPC signal for optically opaque samples is [8]

$$A = \frac{C}{f \sqrt{\cosh(2l_s \sqrt{\pi f / \alpha}) - \cos(2l_s \sqrt{\pi f / \alpha})}} \quad (1)$$

In this expression f is the modulation frequency, α is the thermal diffusivity of the sample, l_s is the sample thickness, and C is a parameter that depends on the pressure, thermal properties of the air inside the acoustic chamber, light intensity, and the cell geometry of the photoacoustic cell. The thermal diffusivity can be obtained by fitting Eq. (1) to signal data amplitude [8, 9].

On the other hand, a study of the microstructure of the samples was carried out using an X-ray diffractometer (Siemens D-5000) and a scanning electron microscope (Philips ESEM-XL30).

3. RESULTS AND DISCUSSION

Experimental results of the thermal diffusivity of our five API5L-X52 low carbon steel samples are given in Table I, showing no significant variations among them and we get an average value of $\alpha = 0.116 \text{ cm}^2 \cdot \text{s}^{-1}$ with an approximately 5% error. Figure 1 shows the PA signal amplitude versus modulation frequency; the curve indicates the best fit of Eq. (1) to the experimental data.

In Table II, α values obtained from the literature [11, 12] for other types of low carbon steel are shown, as well as their compositions in mass percent of C and Mg. After making comparisons, our α value of API5L-X52 steel is 50% less than that of pure iron, 30% less than that of 1018 steel, and 12% less than that of 1020 steel value. Besides this, comparing API-X52 steel with SAE 1010, the C concentration in them is similar ($\sim 0.1\%$), however, the Mg concentration is larger in the API-X52 steel than in the SAE 1010, and the thermal diffusivity is smaller in the API-X52 steel than in the SAE 1010. We deduce a similar behavior when we

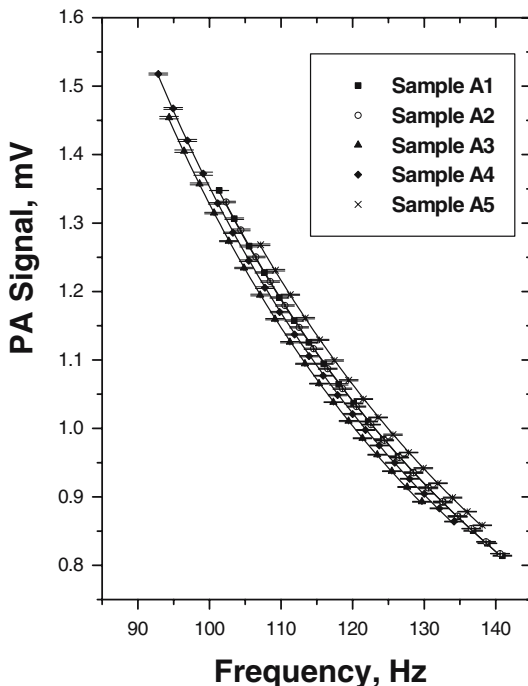


Fig. 1. PA signal amplitude versus frequency, curve indicates the best fit of Eq. (1) to experimental data.

Table II. Thermal Diffusivity for Different Types of Low Carbon Steel [11, 12] at Room Temperature

Samples	C (mass%)	Mn (mass%)	α ($10^{-3} \text{ cm}^2 \cdot \text{s}^{-1}$)
Pure Fe	—	—	227
SAE 1010	0.1	0.42	191
Steel 1018	0.18	~0.50	165
Steel 1020	0.20	~0.60	130

compared samples 1018 and 1020. Therefore, in samples with similar C concentration, we observe that the thermal diffusivity decreases when the Mn concentration increases.

In Fig. 2 we show X-ray diffraction patterns of the API5L-X52 steel samples. The peaks represent the crystalline planes (110), (200), (211), and (220), which correspond to the body-centered-cubic (bcc) structure of the α -Fe phase, with a lattice parameter value of 2.8664 Å. Figure 3 shows the API5L-X52 steel microstructure obtained by means of SEM, with a 500 \times magnification. We can see that the main phase is the α -Fe (b), which is consistent with the XRD results; we can also see small lamellar areas of the pearlite phase (a) and solid inclusions (c). In Fig. 4 we show a 2000 \times magnification of these inclusions (c) with 79.4 particles per mm². Table III presents a quantitative analysis of the inclusions using EDS-SEM. The main elements of these inclusions are Al (33%), Fe (30%), and O (17%). In addition to these, smaller quantities of Mn (8%), S (6.4%), Mg (2.6%), and Ca (2.3%) are shown. Figure 5 shows the corresponding spectrum.

In Fig. 6 is shown the grain size distribution of the α -Fe phase, and the inclusions size distribution is shown in Fig. 7. By means of ASTM E112-96, we obtained values of 6.084 and 3.027 μm for the α -Fe phase and inclusions grain size, respectively.

Table III. Results of Quantitative Elementary Analysis Using EDS-SEM for the Inclusion Particle Observed in Fig. 4

Element	O	Mg	Al	S	Ca	Mn	Fe
(mass%)	17.47	2.60	33.07	6.41	2.27	7.95	30.23

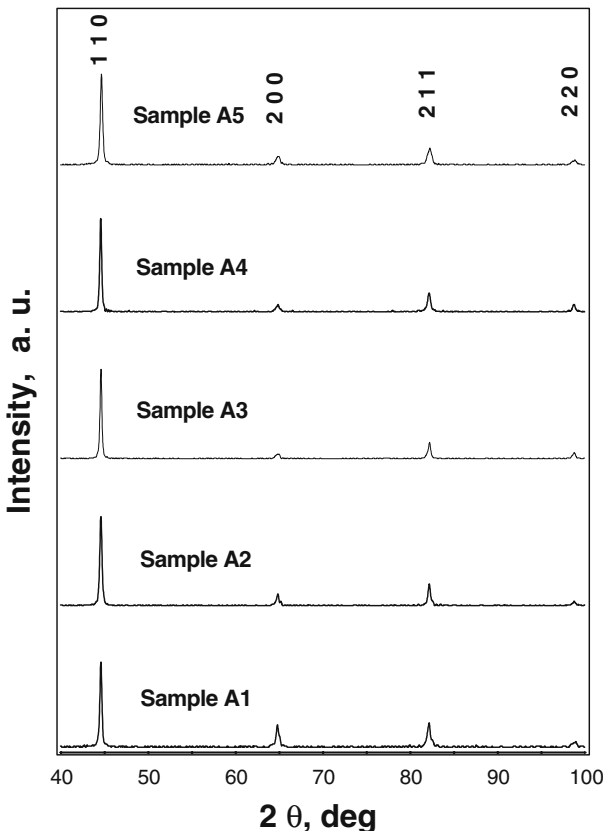


Fig. 2. XRD patterns for API5L-X52 carbon steel samples.

4. CONCLUSIONS

By means of the photoacoustic technique in a heat transmission configuration, we obtained $\alpha = 0.116 \pm 0.006 \text{ cm}^2 \cdot \text{s}^{-1}$ for the thermal diffusivity of API5L-X52 steel at room temperature. Comparing with α values reported in the literature for steels with similar compositions, our measured α for API5L-X52 is 50% less than the α value of pure iron, 30% less than the α value of 1018 steel, and 12% less than the α value of 1020 steel. Moreover, we observed for these samples, and for those with similar C concentrations, that the α value decreases when the Mn concentration increases.

On the other hand, SEM and XRD results are consistent and show that the main phase in API5L-X52 steel is the α -Fe with a lattice

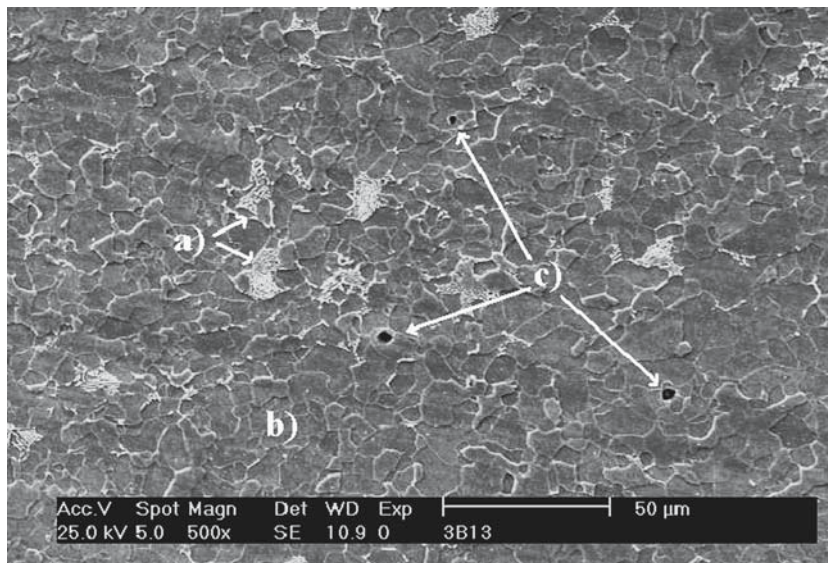


Fig. 3. SEM image showing the microstructure of the API5L-X52 carbon steel by 500 \times magnification: (a) pearlite, (b) ferrite, and (c) solid inclusion particles in the structure (etched in 0.2% nital for 10 s).

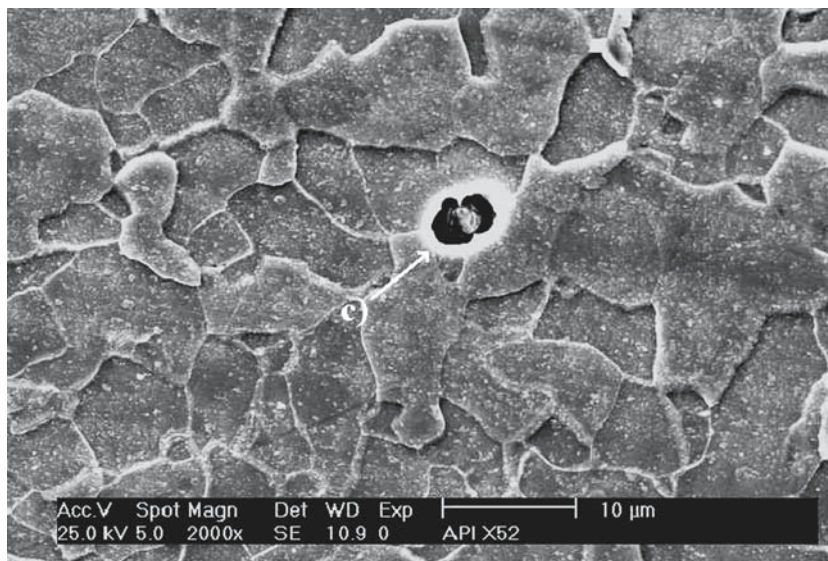


Fig. 4. SEM image showing the microstructure of the API5L-X52 by 2000 \times magnification; micrograph shows a typical solid inclusion particle (c).

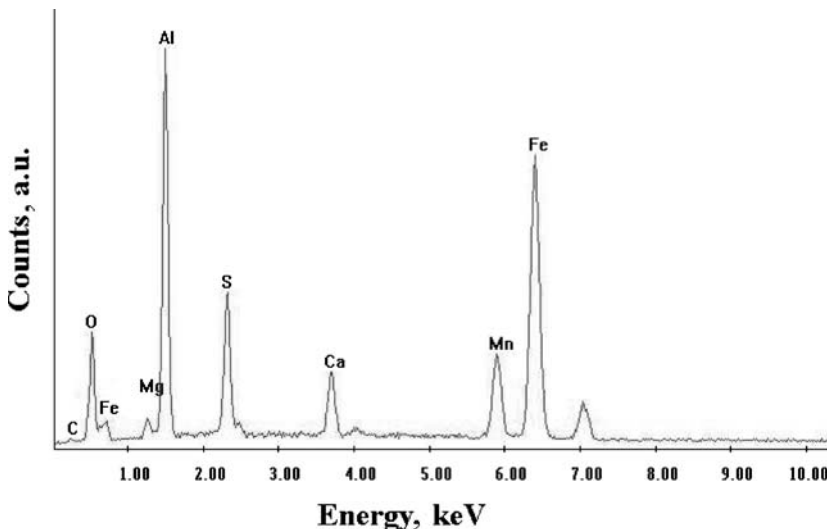


Fig. 5. Spectrum of quantitative elementary analysis using EDS-SEM for the inclusion particle observed in Fig. 4 and presented in Table III.

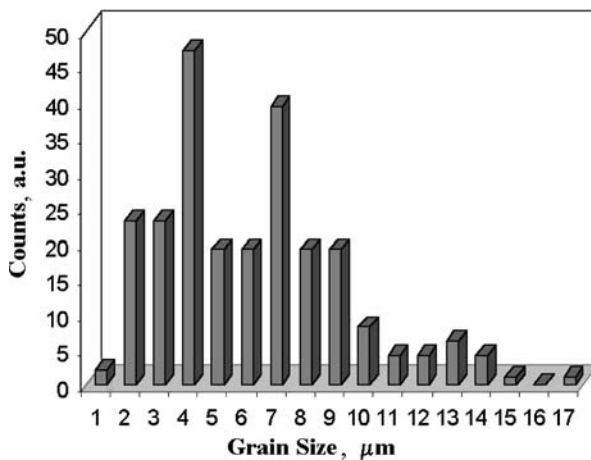


Fig. 6. Grain size distribution for the ferrite phase.

parameter value of 2.87 \AA . The SEM analysis also shows lamellar areas of the pearlite phase and solid inclusions with $79.4 \text{ particles/mm}^2$. EDS-SEM shows that the main elements of these inclusions are Al (33%), Fe (30%), and O (17%) and smaller quantities of Mn (8%), S (6.4%), Mg (2.6%), and

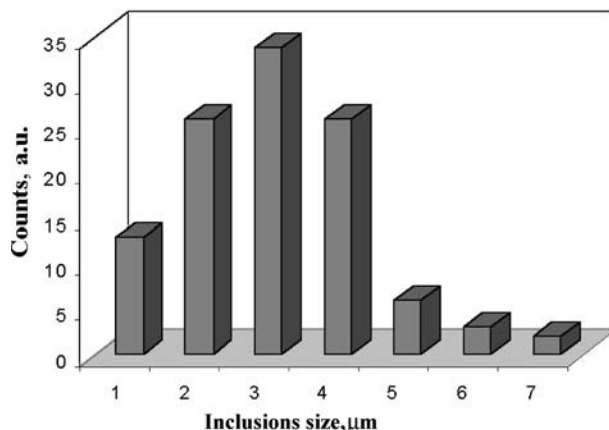


Fig. 7. Distribution of the inclusions size.

Ca (2.3%). The ASTM E112-96 method shows 6.084 and $3.027 \mu\text{m}$ for the α -Fe phase and the inclusions grain sizes, respectively.

ACKNOWLEDGMENTS

The authors would like to thank to Dr. Cheng Dong of the Institute of Physics of the Chinese Academy of Science for giving us permission for the use of the software Powder X. This work was partially supported by Project No. D.000049 of the Instituto Mexicano del Petróleo, CGPI-IPN projects, and the PIFI-IPN program.

REFERENCES

1. D. Fournier, J. P Roger, A. Bellouati, C. Boué, H. Stam, and F. Lakestani. *Anal. Sci.* **17**:s158 (2001).
2. H. G. Walther, D. Fournier, J. C. Krapez, M. LuuKKala, B. Schmitz, C. Sibilia, H. Stamm, and J. Thoen. *Anal. Sci.* **17**:s165 (2001).
3. Yoshihiro Terada, Kenji Ohkubo, Tetsuo Mohri, and Tomoo Suzuki. *Metall. Mater. Trans.* **32 A**:2135 (2001).
4. R. Priestner and A. K. Ibraheem. *Mater. Sci. Tech.* **16**:1267 (2000).
5. P. J. Hurley, G. L. Kely, and P. D. Hodgson. *Mater. Sci. Technol.* **16**:1273 (2000).
6. Private communication, Mike Spanhel, *Upstream Standards*, American Petroleum Institute, 1220 L Street, NW, Washington, DC 20005-4070, E-mail: spanhel@api.org
7. Private communication, Marie T. Brisman, NACE International, Member Service Department, E-mail: marie@mail.nace.org
8. A. Calderón, R. A. Muñoz Hernández, S. A. Tomás, A. Cruz Orea, and F. Sánchez Sinencio. *J. Appl. Phys* **84**:6327 (1998).

9. G. Peña Rodríguez, A. Calderón Arenas, R. A. Muñoz Hernández, S. Stolik, A. Cruz Orea, and F. Sánchez Sinencio, *Anal. Sci.* **17**:s357 (2001).
10. L. F. Perondi and L. C. M. Miranda, *J. Appl. Phys.* **62**:2955 (1987).
11. D. P. Almond and P. M. Patel, *Photothermal Science and Techniques* (Chapman and Hall, London, 1996), pp. 16–17.
12. Y. S. Touloukian, *Thermophysical Properties of Matter*, Vol. 10 (IFI/Plenum, New York, 1973).